PROPULSION MACHINERY OPERATING IN ICE – A MODELLING AND SIMULATION APPROACH

Dražen Polić
Dept. of Marine Technology
HIÅ and NTNU
E-mail: podr@hials.no

Sören Ehlers
Dept. of Marine Technology
NTNU and HIÅ
E-mail: soren.ehlers@ntnu.no

Vilmar Æsøy
Dept. of Marine Technology
HIÅ
E-mail: ve@hials.no

Eilif Pedersen
Dept. of Marine Technology
NTNU
E-mail: eilif.pedersen@ntnu.no

KEYWORDS
Ice-propeller interaction, propulsion machinery response, 20-sim, bond graph, ice strengthened vessel.

ABSTRACT

Shipping activity and offshore operations in Arctic areas are increasing as a result of more effective transportation routes and oil/gas exploration. Vessels navigating in ice covered areas are exposed to additional loads from different ice conditions. In this paper the dynamic loads on propellers are investigated to better understand the impact on propeller, power transmission elements and engine. An ice-propeller interaction model is implemented with a full propulsion machinery to simulate the systems response to ice loads. The ice load models are developed based on the DNV and IACS rules for ice-propellers. Modelling and simulation of interactive multi body systems is a rather complex task, involving hydrodynamics, mechanics, electronics and control systems. This paper describes an approach to link the different models to simulate the overall system response and the interactions between the sub-systems. Therein, the rule-based ice loads are implemented in two ways for comparison: a) a coupled and b) an uncoupled treatment of the ice load and system response. The simulation results show that the dynamic peak loads are 10-20% lower than the maximum peaks predicted by the uncoupled simulation, i.e. conventional rule-based. Simulations also show that the peak loads are damped through the transmission elements, and therefore reducing the load on critical machinery components.

INTRODUCTION

As the amount of vessels capable of navigation in ice-covered waters increases, further understanding of ice-related loads acting on the propeller become important for safe and efficient design and operations of the ice going vessels. Therefore, a simple model of the propulsion machinery is developed to investigate the influence of ice loads on propulsion machinery response. Therefore, DNV and IACS rules for ice strengthened vessels are adopted here to identify the ice loads acting on the propeller. Furthermore, the simulations to be carried out in this paper will focus on merchant vessels with ice class 1A, because this ice class is typically found to be most economic for arctic operations, see Erikstad and Ehlers (2012). Hence, in order to compare IACS and DNV the class notation PC-7 and DNV ICE-1A is utilized, respectively. Further the ice influence described by DNV and IACS rules is extended by relating the ice related loads as a function of angular velocity of the propulsion machinery, i.e. a coupled treatment of the ice loads and system response will be presented.

Propulsion machinery in ice

The propulsion machinery is a coupled system connecting the main engine through a shaft with the propeller to create a directional thrust, see Figure 1. This directional thrust allows the vessel to maneuver and sail in open and ice-covered waters. The latter typically involves the breaking of ice pieces and their submergence in the direction of the water flow around the hull. Consequently, this influences on the hydrodynamic performance of the propeller, because the water inflow to the propeller, i.e. wake field, is disturbed. Furthermore, if a submerged ice piece proceeds further towards the advancing propeller, contact between the ice pieces and the propeller will occur, resulting in an ice-induced contact load. This process is called ice-propeller interaction.

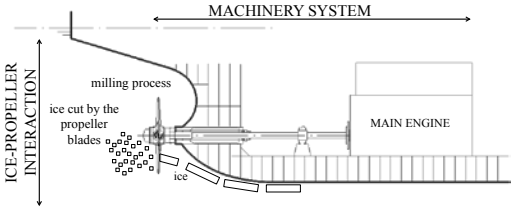

Figure 1: Propulsion machinery in ice

The propeller, being one element of the propulsion machinery, transmits this ice-related contact load together with the hydrodynamic load, being a result of the surrounding water, to the other elements of the propulsion machinery, such as the shaft, flexible and shaft couplings, clutches and gears. In turn, the main

Proceedings 27th European Conference on Modelling and Simulation ©ECMS Webjørn Rekdalsbakken, Robin T. Bye, Houxiang Zhang (Editors)
ISBN: 978-0-9564944-6-7 / ISBN: 978-0-9564944-7-4 (CD)

engine transmits the machinery power to the propeller, which clearly represents a coupled relationship.

Ice-propeller interaction

Veitch (1995) describes the ice-propeller interaction process qualitatively in terms of three stages: approach, blockage and contact. During the approach and blockage stage at least one ice piece is in the path of the advancing propeller. In those conditions, the relative motions between the water and the ice piece as well as the disturbance around the ice piece will increase. This influence is called ice piece wake and it affects only the hydrodynamic performance of the propeller. As the ice moves closer to the propeller the ice piece wake will grow. This growth reaches its maximum just before the ice piece impacts the propeller on the upstream side. Consequently, in the next instance physical contact between the propeller and the ice piece occurs. This contact stage currently defines the strength requirements of the propeller blades and the design load of the propulsion machinery.

The Classification Societies DNV (2012) and IACS (2011) are describing the design load, as a sum of the ice-related contact and hydrodynamic load. The hydrodynamic load is based on open water design parameters. In rules, the torque component of ice-related contact load is defined based on propeller geometrical parameters, angular velocity (rps), and ice thickness and strength. For higher ice class of vessel the ice thickness and strength will grow in the way that thicker ice will have higher strength. The DNV calculation is neglecting the increase in strength by assuming constant strength index of unit value. Except for this the propeller blade thickness is neglected in the ice torque load calculation of the DNV rules. These differences in calculations are presented in equations (1, 2, 3 and 4) in Appendix A. The maximal value of torque is obtained at the maximal allowable rps in ice-covered waters.

The excitation of the torque due to ice-propeller interaction is described with different excitation conditions presented in Table 1. Using the C_q and α_i parameters with maximum torque, equation (1), a single blade impact is described as a half sine shape with function of the propeller rotational advancement:

$$Q(\varphi) = C_q \cdot Q_{\max} \cdot \sin(\pi(\frac{\varphi}{\pi})) \text{ for } \varphi = [0, \alpha_i] \quad (1)$$

$$Q(\varphi) = 0 \text{ for } \varphi = [\alpha_i, 2\pi] \quad (2)$$

where:
Q_{max} – maximum torque [Nm]
φ – propeller rotational position [rad]

Further, number of ice impact is defined as:

$$N = 2 \cdot Z \cdot H_{ice} \quad (3)$$

where:
Z – number of propeller blades
H_{ice} – design thickness of ice [m]

Table 1: Torque excitation factors for different ice cases

Torque excitation	Ice-propeller interaction	C_q	α_i
Case 1	Single ice block	0.5	45°
Case 2	Single ice block	0.75	90°
Case 3	Single ice block	1	135°
Case 4	Two ice blocks	0.5	45°

In Figure 2 the summarized torque component of ice-induced contact load from all blades and with N-numbers of ice impact is presented for case 1, 2 and 3.

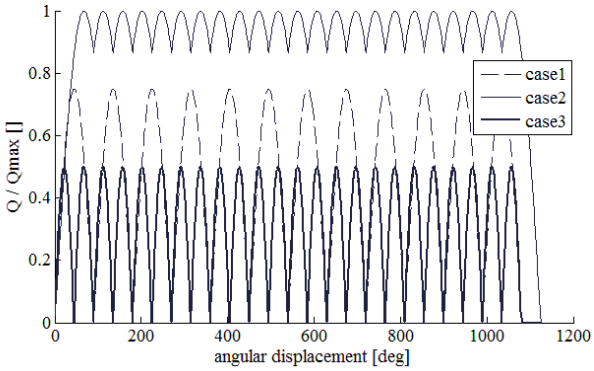

Figure 2: A typical response of the propulsion machinery during ice-propeller interaction for a four-bladed propeller in 1.5 m thick ice (IACS)

Furthermore, in this paper only case 2 and 3 are analysed, because the influence of the ice related load is most dominant here. Additionally, case 4 for is essentially equal to case 1, however, having twice the amount of ice block impacts following two ice blocks impacting the propeller. Further, DNV neglects case 1 entirely due to its low significance and generally utilizes a linear ramp function for 270° of propeller advancement at beginning and at the end of the ice-propeller interaction (see also Figure 7 and 8 for comparison of DNV and IACS). This makes the first two impacts of ice, in the case of propeller with four blades, less impulsive than for the IACS rules, which increase the load with the first impact to the full load level. Common for both rules, is that the torque excitation is given as a function of maximum allowable propeller angular velocity. This assumes a constant propeller angular velocity and thus the coupled relationship between the propeller and the engine is neglected. On the top of this the hydrodynamic torque needs to be added as well as the dynamic response of the propulsion machinery.

Therefore, a dynamic simulation model is developed using the same parameters and equations as described by the rules above, but with a propeller torque as function of the propulsion machinery response. Using this approach the angular velocity and angular position of the propeller are considered in calculation of the torque excitation. The influence of the torque excitation

in the coupled simulation due the propeller angular velocity drop from ω_1 to ω_3 during a single ice impact is illustrated in Figure 3. Further, the growth at the end of a single ice impact will depend on the dynamics of the main engine.

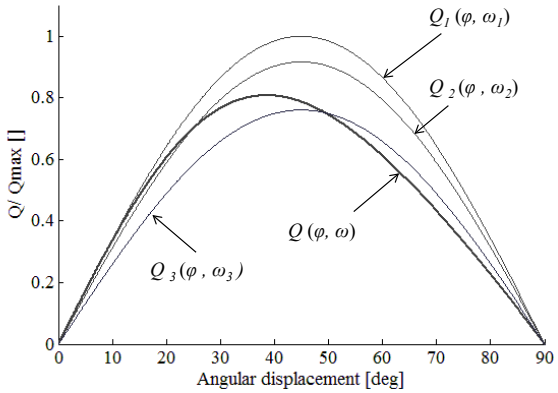

Figure 3: Simplified comparison of uncoupled $Q(\varphi,\omega_{1..3})$ and coupled $Q(\varphi,\omega)$ simulation for a single ice impact

Power transmission system

The most common and most efficient transmission systems are mechanical connections between the propeller and engine shaft. Mechanical transmissions are modelled as a multi-body system, consisting of a series of rigid bodies connected through various types of flexible joints. For long shaft lines a modal model is applied to include the higher order oscillations. Typical constraints to these flexible elements are: dynamic stress causing fatigue problems and maximum allowable angular deformations of shaft 0.2 – 0.4 deg/m and flexible couplings up to 30 deg/m.

To protect critical components from the dynamic stress and fatigue, the overall system must be analysed and designed in a holistic fashion. Dynamic overload can be avoided through shock absorbing elements such as flexible coupling, or even by introducing a weak link which is easy to repair in case of overload.

Main engine

The engine layout analysed in this paper is the most common solution for merchant ships. Typical constraints to the diesel engine are: 1) only one source of propulsion power; 2) engine designed for open water steady state operations; 3) engine dynamic is dependent on the ice-propeller interaction; 4) engine is directly exposed to the dynamical loads from ice-propeller interaction, causing irregularities in working operation and possible torsion vibrations which can damage the mechanical parts and cause thermal stress and fatigue; 5) rapid load variations also cause combustion problems resulting in thermal stress, soot formation, and unwanted exhaust gas emissions; 6) engine torque and speed limitations may cause stop and start problems caused by blocking ice.

MODELING

The developed mathematical model, which will be used for the simulation of the dynamic response of the propulsion machinery, consists of the following: a fixed pitch propeller (FPP) in direct connection to a low-speed engine through a shaft and a flexible coupling, see Figure 4. This arrangement is energy efficient, robust and hence the most common solution for merchant vessels. All elements of the propulsion machinery are modelled in the 20-sim-software Version 4.3 and presented as sub-models in Figure 4. The bond graph method is used to describe the power transfer and energy flow between the corresponding sub-elements and within the components of the sub elements as the product of effort (e) and flow (f). In bond graph terminology these two variables are called power variables. Additionally, the generalised momentum (p) and displacement (q) are called energy variables. Consequently, the energy supply is presented as effort (S_e) or flow (S_f), while the energy storage as momentum (I) and displacement (C), see Figure 5. The energy dissipation is presented as a resistor (R). Furthermore, to enable interaction between these system components we need to introduce power element TF and junction elements 1 and 0. A transformer is an element which transforms an effort on one port into an effort on the other port with some magnitude m, while a junction element is an ideal power transmitter, which transmits power instantly between ports without storing or dissipating energy. Further, the *0*-junction represents geometric compatibility, while the *1*-junction represents a dynamic force balance. For further details please see, for example, Karnopp et al. (2005) and Pedersen and Engja (2010).

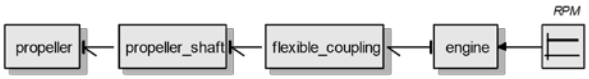

Figure 4: FP propeller directly coupled with engine

In the present model effort, flow, momentum and displacement are representing torque, angular velocity, angular momentum and angular displacement (angle), respectively. Further, the S_e-, I-, C- and R-elements present respectively the main engine as a source of torque, the moment of inertia, a torsional stiffness and the propeller as energy consumers. Additionally, the connections between these elements are represented with a *1*-junction if the velocity is equal otherwise with a *0*-junction. Additionally, the relationship for the energy transfer between and within these system elements of the bond graph representation needs to be derived. The latter is presented in the following sub-chapters.

Propeller

The propeller is described through its moment of inertia and its resistance. In bond graph terminology, this relates to the I- and R- element, respectively. The constant propeller moment of inertia is calculated based on its geometrical parameters, while the propeller

resistance is obtained based on the angular velocity. The latter is equal for both elements and thus allows their connection with a *1*-junction. Together, these three elements are used to describe the propeller torque in ice as follows: 1) the *1*-junction element transmits the effort (*e*), i.e. torque, from the propulsion machinery to the propeller; 2) under the assumption of linear dependency, between the propeller and the remainder of the propulsion machinery, this effort is distributed between the *I*- and *R*- elements; and 3) a flow response is derived as a function of effort and the propeller inertia.

Transmission system model

Power transmission between the FPP and the low-speed engine is realized with a so-called directly coupled system using a shaft and a flexible coupling. Therein, the shaft is modelled as a system of finite lumps or modes deduced from a modal decomposition of the continuous representation of the shaft. Following the bond graph concept a combination of the latter is possible (see Margoli et al. 1977, Karnopp et al. 2000) which also allows a reduction of the model extent without simulation accuracy loss. In order to do so, the natural frequencies and modes of the system must be maintained (see Margoli et al. 1977, Karnopp et al. 2000, Valland 1999). Considering the latter the mode shapes of the shaft were evaluated at the location of the torque and added inside *TF* element as a magnitude m = 1. The only exception is a *TF6* element, where m = -1 due to shape of the mode 2 and torque location $x = L$. Further, for each mode the modal shaft stiffness (C), mass (I) and damping (R) is calculated using the initial propeller position as a shaft origin.

Since the present flexible coupling is a short element, only few modes and natural frequencies exist. However, its dynamic properties must be approximated with sufficient accuracy, i.e. the stiffness of the rubber material or the hydrodynamic damping arising from the oil inside the flexible coupling. Using *C*- and *R*-elements those dynamic properties are included and connected to a *0*-junction. The reason for the latter arises from the change in flow and angular velocity over the shaft length, while the amount of effort, i.e. torque, is constant over the entire cross-section.

Engine model

A simplified model of the diesel engine is applied in this study Figure 5. The combustion process is modelled as a torque source (*MTF*) supplying power from the engine speed controller signal to the crank shaft, represented by a single inertia element (I). Mechanical friction is modelled as a resistor (R). The PID angular velocity governor, proportional-integral-derivative controller, is controlling the fuel injection limited by the engine operational constraints. As a result, the response angular velocity output from this simplified engine system is derived and compared with the angular velocity reference input. The torque input are controlled within a range of 10% to 110% of its maximum value, which is given as a function of angular velocity.

Propulsion machinery model

In Figure 3 the combined bond graph of each sub system is shown representing the entire propulsion machinery model.

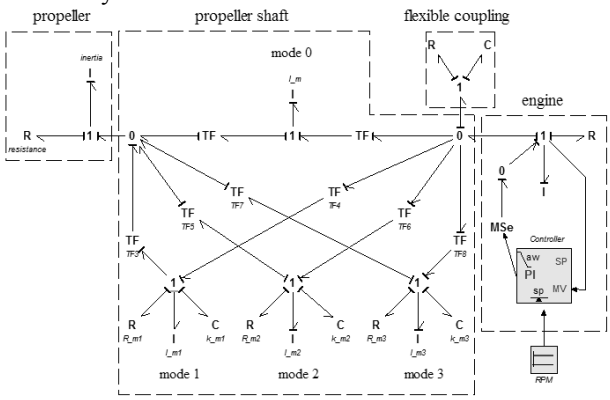

Figure 5: Overall bond graph model of the propulsion machinery system

RESULTS

Using the propulsion machinery model described in the previous chapter uncoupled and coupled response simulations for ice-propeller interaction are carried out. Coupled simulations includes the dynamic response of the entire machinery, while uncoupled is the load when propeller is assumed to run at constant speed without dynamic response. In order to do so, the required propeller geometry and efficiency diagram as well as the resistance in ice is selected from Lee (2008) for the case study vessel. Therefrom, the four-bladed propeller rpm are obtained for a selected sailing speed of 5 knots in 1.5m thick ice as well as the related hydrodynamic load acting on the propeller in open water at this rpm rating. Furthermore, based on the required rpm for maximum open water speed we selected an appropriate engine that delivers the required power for navigation in ice. Additionally, the damping and stiffness of the flexible coupling, see Figure 5, as well as the shaft diameter is defined based on the design load defined in the ice-propeller interaction chapter. The details are given in appendix A/B. Therein also the engine controller parameters, used in this study, are presented.

The results of the simulation are presented in Figure 6, 7 and 8, and they describe the distribution of the torque load for case 2 and 3 of the ice-propeller interaction simulations. In Figure 2 a coupled simulation of the propulsion machinery is presented for case 2 and 3 with normalized values of torque load and the propeller angular velocity, presented as revolutions per minute (rpm). Therein, it can be seen that both cases show comparatively small differences, even though 75% of the maximum ice related load is applied in case 2; see parameter Cq in Table 1; while 100% of the maximum ice-related contact load are applied in case 3. The reason

for this similarity in torque in spite of the ice related load difference arises from the increase of the hydrodynamic load in case 2. Therein, the hydrodynamic load is a function of the propeller rpm's being a function of the system response in turn. The relationship between this hydrodynamic load and the propeller rpm's is given in appendix A/B of this paper.

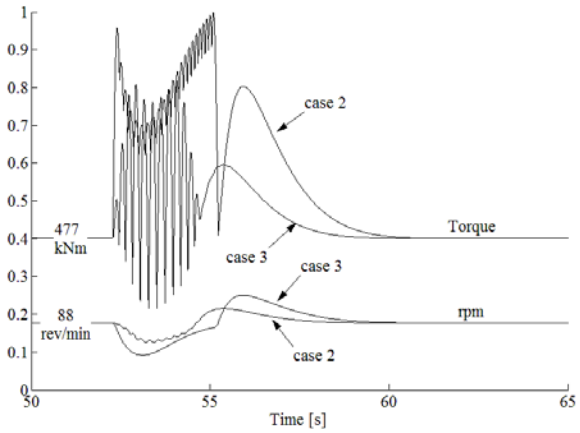

Figure 6: A typical response of the propulsion machinery during the milling of a single ice block

The largest influence of the ice on the propeller load is found in case 3, which is therefore presented in Figure 7 and 8 for DNV and IACS, respectively. These figures include, besides the load for the coupled and uncoupled simulation, the hydrodynamic and ice-related contact load for comparison. Thereby it can be seen that the ice-related contact load is nearly constant during the ice-propeller interaction while the deviation of the coupled load is caused by the change in hydrodynamic load. Furthermore, a difference between the ice-related coupled and uncoupled contact load can be identified.
Most importantly however, it can be seen in Figure 7 and 8 that the load in a coupled simulation is lower, except last two ice impacts with the linear ramp function described by DNV, than the load in an uncoupled simulation. The reason for this is the dependency of the coupled load, consisting of the hydrodynamic and ice-related contact load, on the propeller rotational speed. The latter decreases once ice impacts the propeller, which consequently causes a reduction in coupled load. However, after this initial impact and speed reduction the machinery system accelerates and thus increases the coupled torque, in the current example above the initial ice-impact load level. The latter however depends on the engine capabilities, since only an engine with additional power reserve is capable to compensate and accelerate further, in case this reserve is not available, the propeller will be blocked by the ice and the rps's drop to zero.

To present the influence of the coupled or uncoupled simulation further, Table 2 compares case 2, triangular shaped ice-related contact load, with case 3, which has a cumulatively increasing ice-related load as shown in Figure 2. The resulting difference between these cases is shown by means of maximum torque value for the uncoupled and coupled simulations, respectively. The uncoupled simulation results in higher torque values since the load is independent from propeller angular velocity.

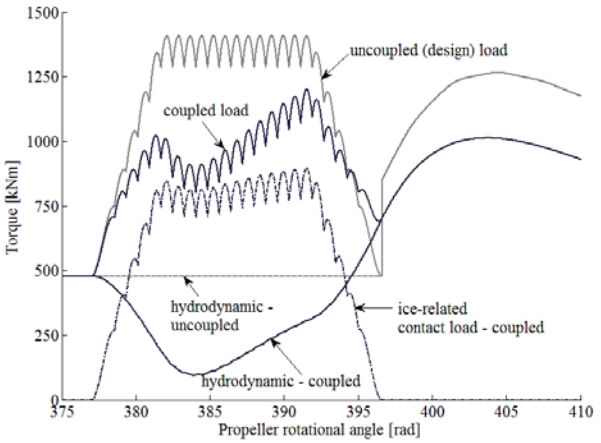

Figure 7: Comparison of the propeller response for the uncoupled and coupled DNV torque for case 3

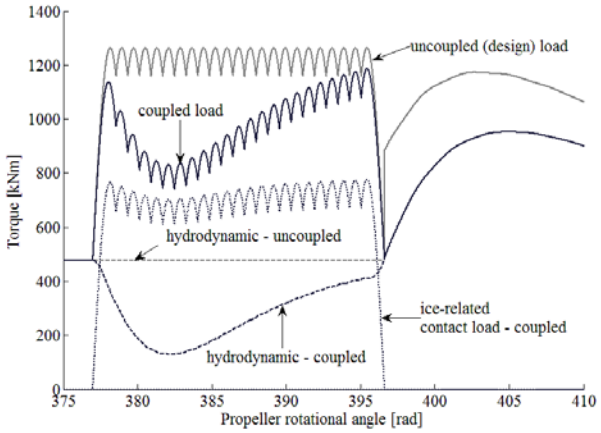

Figure 8: Comparison of the propeller response for the uncoupled and coupled IACS torque for case 3

Table 2: Comparison of uncoupled and coupled (*) design torque of the ice-propeller interaction for case 2 and case 3.

	Case 2	Case3
	max Q [kNm]	max Q [kNm]
DNV (100%)	1180	1410
DNV*	83%	85%
IACS	91%	90%
IACS*	85%	84%

In addition to the presented differences for the coupled and uncoupled simulations, the presented model can be used to analyse the load acting on different components of the machinery system. Hence, we can identify the deformation of shaft and a flexible coupling element caused by the excitations of the design load. Therein, the deformation magnitude is defined by the amplitude and shape of the loading, which was found to be higher for case 3, see Figure 9. In case 2, where the steep initial slope of the design load applied causes the deformations

grow rapidly. This growth of deformation $\Delta\dot{\theta}$ per single ice block impact is presented in Table 3 and 4 for an interval of 0.1s. Therein, the results are given relative to the base case set by the DNV loading and a simple multiplication of the deformation growth with the duration Δt will result in the maximum deformation per ice impact. Furthermore, it can be stated that the steep initial slope at the beginning and at the end of the milling sequence, described by IACS, causes a higher deformation growth. In all cases, the deformation and deformation growth are 10 to 20% lower in the coupled simulation compared to the uncoupled simulation.

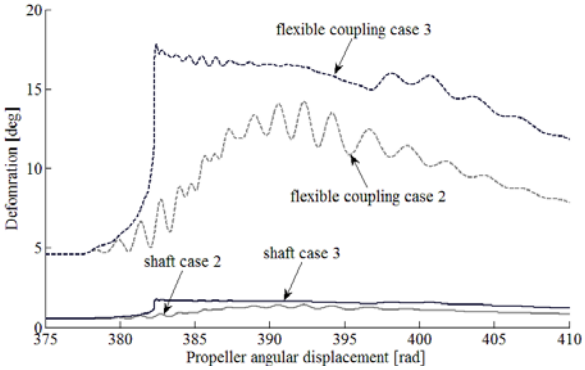

Figure 9: Comparison of the twist angle in shaft and flexible coupling for uncoupled DNV case 2 and 3

Table 3: CASE 2 - Influence of the uncoupled and coupled (*) simulations on the deformations of the shaft, θ1, and the flexible element, θ2.

	max θ_1 [deg]	max $\Delta\dot{\theta}_1$ [deg/s]	Δt_1 [s]	max θ_2 [deg]	max $\Delta\dot{\theta}_2$ [deg/s]	Δt_2 [s]
DNV (100%)	1.42	0.25	0.11	14.22	2.69	0.11
DNV*	73%	111%	97%	71%	112%	96%
IACS	93%	101%	101%	92%	101%	102%
IACS*	75%	120%	86%	72%	118%	88%

Table 4: CASE 3 - Influence of the uncoupled and coupled (*) simulations on the deformations of the shaft, θ_1, and the flexible element, θ_2.

	max θ_1 [deg]	max $\Delta\dot{\theta}_1$ [deg/s]	Δt_1 [s]	max θ_2 [deg]	max $\Delta\dot{\theta}_2$ [deg/s]	Δt_2 [s]
DNV (100%)	1.75	0.05	0.10	17.80	0.54	0.10
DNV*	81%	123%	140%	80%	115%	164%
IACS	96%	225%	144%	96%	218%	149%
IACS*	76%	216%	127%	75%	209%	132%

Further, the torque in the shaft and flexible coupling element is analysed and compared with propeller load. The largest influence is found in uncoupled simulation of DNV case 2 and case 3, which is therefore presented in Figure 10. Thereby it can be seen that the torque difference in shaft and flexible coupling is insignificant and the reason is in the small angular velocity of propulsion machinery and shaft inertia. However the most important is to see a delay in the torque between the propeller and power transmission elements caused by propeller inertia. Particularly in this case, propeller has ten times higher moment of inertia than the power transmission elements. Furthermore, in all cases the torque maximum value is higher inside power transmission elements than the torque experienced by the propeller.

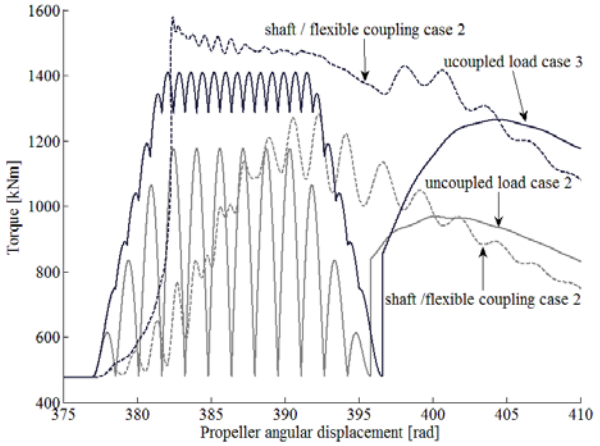

Figure 10: Comparison of the torque in shaft and flexible coupling with propeller load for uncoupled DNV case 2 and 3

SUMMARY AND DISCUSSION

This paper presents dynamic response of the propulsion machinery in ice. A simple model was developed to identify the influence of ice-propeller interaction also introducing an uncoupled and coupled simulation. DNV and IACS rules where used to calculate the propeller torque load, and angular velocity. As a result, maximum values of torque and angular deformation indicate that the uncoupled simulation is more conservative and thus may lead to over dimensioning of the machinery system. Furthermore, the coupled simulation highlights the necessity to consider the dependency between the propeller design load and angular velocity of propulsion machinery. However, this coupled simulation needs to be extended further to identify the validity of the rule-based ice-related loads and the accuracy of the engine response. In other words, the dependency of the propulsion machinery, especially power transmission system, on the hydrodynamic and ice-related contact load must be investigated further. Furthermore, the ice-propeller loads need to be related to actual ice properties, while the main engine acceleration and power with the actual combustion process. Additionally, the simulation approach shall be extended to include medium-speed engines coupled to the propeller shaft by a reduction gear, or electric motor(s) driving the propeller using power from the diesel generators. In conclusion, the present study forms a basis for the evaluation of the current design load and propulsion machinery scantling determination for ice going vessels.

ACKNOWLEDGEMENTS

This research is funded through the Norwegian Research Council project.no.194529

REFERENCE

DNV rules. 2012. “Ships for Navigation in Ice.”

Erikstad, S.O.; Ehlers, S. 2012. “Decision Support Framework for Exploiting Northern Sea Route Transport Opportunities”, Journal for Reserch in Ship Technology, Vol. 59, No. 3. 34 – 43.

IACS rules. 2011. “Requirements Concerning Polar Class.”

Karnopp, D.C.; Margolis, D.L. and R.C. Rosenberg. 2005. “ System Dynamics - Modelling and Simulation of Mechatronic Systems.” John Wiley & Sons Inc., Fourth edition.

Lee, S.K. 2008. “Combining Ice Class Rules with Direct Calculations for Design of Arctice LNG Vessel Propulsion.” Gastech conference proceedings 2008.

Margolis, D.L.; Young, G.E. 1977. “Reduction of Models of Large Scale Lumped Structures Using Normal Modes and Bond Graphs.” Journal of the Franklin Institute, Vol. 304, No.1.

Pedersen, E.; Engja, H. 2010. “ Lecture Notes in TMR4275 Modelling, Simulation and Analysis of Dynamic Systems.” NTNU.

Valland, H. 1999. “Analysis of Torsional Vibration in Branched Shafting Systems.” The TORSIO system, Computational Methods. NTNU, Dept. of marine engineering, Trondheim.

Wilson, C.E. 1997. “Computer Integrated Machine Design”, Prentice-Hall International.

Veitch, B. 1995. “Prediction of Ice Contact Forces on a Marine Screw Propeller During the Propeller-Ice Cutting Process.” PhD thesis, Acta Polytechnica Scandinavica, Finland.

APPENDIX A

DNV and IACS equations for propeller torque calculation. Maximal torque on a propeller due to ice influence is equal to:
Q_{max} is the maximum ice-related torque on a propeller.
For $D < D_{limit}$

$$Q_{max\_DNV} = 7.7 \cdot (1 - \frac{d}{D}) \cdot \left(\frac{P_{0.7}}{D}\right)^{0.16} \cdot (nD)^{0.17} \cdot D^3 \quad (1)$$

$$Q_{max\_IACS} = 105 \cdot (1 - \frac{d}{D}) \cdot S_{qice} \cdot \left(\frac{P_{0.7}}{D}\right)^{0.16} \cdot (\frac{t_{0.7}}{D})^{0.6} \cdot (nD)^{0.17} \cdot D^3 \quad (2)$$

For $D \geq D_{limit}$

$$Q_{max\_DNV} = 14.6 \cdot (1 - \frac{d}{D}) \cdot \left(\frac{P_{0.7}}{D}\right)^{0.16} \cdot (nD)^{0.17} \cdot D^{1.9} \cdot H_{ice}^{1.1} \quad (3)$$

$$Q_{max\_IACS} = 202 \cdot (1 - \frac{d}{D}) \cdot S_{qice} \cdot \left(\frac{P_{0.7}}{D}\right)^{0.16} \cdot (\frac{t_{0.7}}{D})^{0.6} \cdot (nD)^{0.17} \cdot D^{1.9} \cdot H_{ice}^{1.1} \quad (4)$$

with:

$$D_{limit} = 1.8 \cdot H_{ice} \quad (5)$$

d – external diameter of propeller hub [m]
D – propeller diameter [m]
S_{qice} – ice strength index for blade ice torque
$P_{0.7}$ – propeller pitch at 0.7 radius at MCR in free running conditions [m]
$t_{0.7}$ – maximal thickness at 0.7 radius [m]
n – propeller rotational speed [rev/s]
H_{ice} – maximum ice block thickness [m]

APPENDIX B

LNG vessel DNV ICE 1A with twin screw
L = 200 m // length
B = 28 m // breadth at water line
T = 9 m // maximal draft
V = 40 000m^3 // cargo capacity
w = 0.143 // wake factor
v_{ow} = 17 kn// vessel open water speed
v_{ice} = 5 kn // vessel speed in ice
R_{ow} = 1192.5 kNm // vessel total resistance at v_{ow}
R_{ice} = 2 157.8 kNm // vessel total resistance at v_{ice}

Ice class parameters
H_{ice} = 1.5m // ice thickness
S_{qice} = 1 // ice strength index for torque

Propeller parameters
D = 6m // propeller diameter
d = 1.8m // external diameter of propeller hub
$P_{0.7}$ = 4.2m// propeller pitch at 0.7R
$t_{0.7}$ = 0.1016m // maximal blade thickness at 0.7R
EAR = 0.55 // expended area ratio
J_p = 46000 kgm^2 // propeller inertia
RPM = 88 // propeller rpm’s needed at v_{ice}
RPM_ow = 102 // propeller rpm’s needed at v_{ow}
Q_{ow} = 640.36 kNm // propeller torque required at open water conditions at v_{ow}
Relationship between propeller rpm and hydrodynamic torque:

$$Q_{ow} = L_{ow} \cdot abs\ (RPM_{ow}) \cdot RPM_{ow} \quad (1)$$

L_{ow} = 5618.43 kNm/s^2 // propeller loading coefficient

Shaft parameters
L_{shaft} = 10 m // shaft length
G = 78 GPa // shear modulus for steel
ρ = 7800 kg/m^3 // steel density
T = 1410 kNm // max torque
N_{sf} = 3.5 // factor of safety
S_{yd} = 655 MPa // steel yield stress
d_{shaft} = 0 m // shaft inner diameter
Using Von Misses Stress criteria and safety parameters, given in (Wilson 1997), shaft diameter is calculated using equation:

$$D_{shaft} = \left(\frac{32 \cdot \sqrt{3} \cdot T \cdot N_{sf}}{\pi \cdot (1 - \frac{d_{shaft}}{D_{shaft}}) \cdot S_{YP}}\right)^{\frac{1}{3}} \quad (2)$$

D_{shaft} = 0.5 m // shaft diameter

Flexible coupling
C_{Tstat} = 4.78 MNm/rad // static stiffness
ω = 46 rad/s // phase velocity of vibration
ω_0 = 690 rad/s // characteristic coupling frequency

$$\kappa = 0.02 + 1.1\frac{\omega}{\omega_0} \quad (3)$$

κ = 0.09 // undimensioned damping factor

$$k = \frac{\kappa \cdot C_{Tstat}}{\omega} \quad (4)$$

k = 9.711 kNms/rad // linear viscous damping

Engine (2 - stroke)
Type 2 – stroke
J_e = 5060 kgm^2// Engine (crank shaft) inertia
RPM*= 105 // engine rated rpm
P = 11.3 MW // engine power in ice
P* = 13.3 MW // engine rated power
η_m = 0.8 // mechanical efficiency

Engine controller
Type PI – controller (20-sim reference PI_sp_aw)
κ = 0.005 // proportional gain
T_i = 0.1 s // Integral time constant
b = 0 // proportional set point weighting parameter
T_a = 1 s // tracking time constant
$minimum$ = 0.1 // minimum controller output
$maximum$ = 1.1 // maximum controller output

Simulation parameters
n_{b_ice} = 60 // number of blade revolutions before ice contact
t_{simu} = 0.1 ms // time step of simulation
Method BDF // backward differential formula